Nucleic Acids Research, 1994, Vol. 22, No. 16 3293–3303

Parallel-stranded duplex DNA containing blocks of *trans* purine – purine and purine – pyrimidine base pairs

Elisabeth M.Evertsz, Karsten Rippe+ and Thomas M.Jovin*
Department of Molecular Biology, Max Planck Institute for Biophysical Chemistry, PO Box 2841, D-37018 Goettingen, Germany

Received June 27, 1994; Revised and Accepted July 25, 1994

ABSTRACT

A 30 base pair parallel-stranded (ps) duplex ps-L1·L2 composed of two adjoined purine – purine and purine – pyrimidine sequence blocks has been characterized thermodynamically and spectroscopically. The 5′-terminal 15 residues in both strands ('left-half') consisted of the alternating $d(GA)_7G$ sequence that forms a ps homoduplex secondary structure stabilized by d(G·G) and d(A·A) base pairs. The 3′-terminal 15 positions of the sequence ('right-half') were combinations of A and T with complementary reverse Watson – Crick d(A·T) base pairing between the two strands. The characteristics of the full length duplex were compared to those of the constituent left and right halves in order to determine the compatibility of the two ps helical forms. The thermal denaturation curves and hyperchromicity profiles of all three duplexes determined by UV absorption spectroscopy were characteristic of ps-DNA, in accordance with previous studies. The thermodynamic properties of the 30 bp duplex corresponded within experimental error to the linear combination of the two 15-mers. Thus, the T_m and ΔH_{vH} of ps-L1·L2 in 10 mM $MgCl_2$, derived from analyses according to a statistical mechanical formulation for the helix – coil transition, were 43°C and 569 kJ mol^{-1}, compared to 21°C, 315 kJ mol^{-1} (ps-F5·F6) and 22°C, 236 kJ mol^{-1} (ps-GA_{15}). The UV absorption and CD spectra of ps-L1·L2 and the individual 15-mer ps motifs were also compared quantitatively. The sums of the two constituent native spectra (left + right halves) accurately matched that of the 30 bp duplex, with only small deviations in the 195 – 215 nm (CD) and 220 – 240 nm (absorption) regions. Based on analysis by native gel electrophoresis, the sequences studied formed duplex structures exclusively; there were no indications of higher order species. Chemical modification with diethyl pyrocarbonate showed no hyperreactivity of the junctional bases, indicating a smooth transition between the two parallel-stranded conformations. We conclude that under given salt conditions, oligonucleotides with normal primary chemical structures can readily form a parallel-stranded double helix based on blocks of very disparate non-canonical purine – purine and purine – pyrimidine base pairs and without perceptible destabilization at the junction. There are biological implications of these findings in relation to genetic structure and expression.

INTRODUCTION

Numerous studies have established that DNA strands have the capacity to adopt a parallel orientation in stable hydrogen-bonded structures with a duplex, triplex, or tetraplex stoichiometry. Most parallel-stranded (ps) DNA and RNA quadruplexes reported to date have been restricted to purine sequences rich in guanine (G) (1–4). In contrast, all four nucleotides can be accommodated in some type of a parallel-stranded duplex. Acidic conditions favoring the protonation of cytosine (C) or (at lower pH) adenine (A) lead to the formation of ps DNA and RNA homo- and heteroduplexes with polymers (5,6) and oligonucleotides (7,8). At neutral pH, the secondary structure of duplex ps-DNA is stabilized by d(A·T) and d(G·C) base pairs (reviewed in 9–12), and additional base pairing schemes have been proposed (13–15). The first experimental verification of ps purine–pyrimidine DNA (ps_{RY}-DNA) proposed by Pattabiraman (16) and Kuryavyi (14) was derived from work with oligonucleotide hairpins (17) and duplexes (18,19). Investigations with natural sequence DNA have provided additional evidence for stable ps structures (20,21).

Much of our recent work in this area has been with a 'D-series' of 25 bp oligonucleotides composed of A and T (22). This set of 4 oligonucleotides combined to make two pairs of parallel and anti-parallel duplexes. Derivatives with G·C (23) and U·A (24) substitutions have also been investigated. These sequences were designed to confer a high selective stabilization of the fully paired ps orientation as opposed to all alternative partially paired anti-parallel structures (12). The D-series and related oligonucleotides have been extensively characterized by thermodynamic and spectroscopic analysis, as well as chemically and biochemically

*To whom correspondence should be addressed

+Present address: Institute of Molecular Biology, University of Oregon, Eugene, OR 97403, USA

using a variety of modification, ligand binding, and enzymatic techniques (12,22,23,25–33). The ps orientation was established by fluorescence measurements of resonance energy transfer (fluorescein/tetramethylrhodamine donor–acceptor pair) (9,30) and excimer formation (pyrene dimers) (12,13,30,32) in duplexes of two end-labeled strands. Furthermore, ^{1}H-NMR (34), Raman (28) and infrared (31) spectroscopy have verified the existence of *trans* reverse Watson–Crick d(A·T) base pairs in ps_{RY}-DNA. The sugar conformation is primarily C2′ *endo*, the glycosyl orientation *anti*, and the helical sense right-handed (27,28). ps_{RY}-DNA is characterized by distinctive UV absorption and CD spectra, and thus by a hyperchromicity pattern upon thermal denaturation differing significantly from that of aps B-DNA (9,17–20,22,26,35,36).

Stable ps purine–purine homoduplexes (ps_{RR}-DNA) formed at neutral pH from synthetic oligonucleotides containing only the purines G and A have been reported recently (13). The technique based on pyrene excimer fluorescence was introduced to establish the parallel-stranded orientation of the two identical strands. The secondary structure in such duplexes formed from the alternating $d(GA)_nG$ sequence is based on trans d(A·A) and d(G·G) base pairs and is preferentially stabilized by Mg^{2+} ions. ps_{RR}-DNA displays distinctive UV absorption and CD spectral characteristics (13), and its ps orientation has been further confirmed in a recent study by a novel psoralen crosslinking technique applied to molecules containing a single potential crosslinking site at the 3′ end (37). Models derived from force-field calculations, and the spectroscopic and chemical modification data demonstrate that the overall conformation of ps_{RR}-DNA is distinct from that of ps_{RY}-DNA but the molecules are similar in thermodynamic stability.

The above studies have established that both ps_{RR}-DNA and ps_{RY}-DNA are stable, alternative forms of ps duplex DNA. The proliferation of known sequence motifs capable of adopting the ps double helical conformation increases the scope of potential biological functions (12,20). An exploration of such possibilities, however, requires detailed knowledge as to which ps conformations can be incorporated singly or in combination into stable duplexes under physiological conditions. The present study addresses the mutual compatibility of the ps_{RR} and ps_{RY} double helices within a single fragment of DNA. Fifteen purine–purine base pairs were juxtaposed to 15 d(A·T) base pairs, creating a novel ps-duplex containing three out of the four naturally occurring bases. The 30-mer is stable at neutral pH and moderate salt concentration and its properties are predicted to a remarkable degree by the superposition of the two constituent segments.

MATERIALS AND METHODS

Oligonucleotide synthesis and gel electrophoresis

The oligonucleotides used in this study (Fig. 1) were synthesized by conventional phosphoramidite chemistry with an Applied Biosystems Model 381A DNA synthesizer. Purification was performed as described previously (22) with reverse phase HPLC using a C18 column before detritylation. The DNA was detritylated, desalted using Waters Sep-Pack cartridges, and fractionated on a Pharmacia Mono Q HR5/5 anion-exchange column. The concentration of DNA was determined using extinction coefficients derived from previous studies and refined by spectral fitting operations described under Results. The values at 260 nm and 70°C (in 10 mM $MgCl_2$) were (mM base^{-1} cm^{-1}): L1 + L2, 10.6; F5 + F6, 10.3; GA_{15}, 10.9. DNA oligonucleotides were radioactively labeled for gel electrophoresis using T4 phage polynucleotide kinase (New England Biolabs) and [γ-^{32}P]ATP. Native gel electrophoresis was performed with 15% polyacrylamide (19:1 monomer/crosslinker) at 7°C. The reservoir and gel buffer was Tris–borate, pH 8.0, 10 mM $MgCl_2$. Autoradiographs were made with Kodak XAR film. Gel Figure 2B was generated with a PhosphorImager SF (Molecular Dynamics).

Chemical modification with diethylpyrocarbonate

Reactions were performed in 100 μl solutions containing 0.5 μM duplex, radioactively labeled on either the DL1 or DL2 strand, 10 μl DEPC in 10 mM $MgCl_2$, 45 mM Tris–borate, pH 7, buffer incubated on ice. Oligonucleotides were modified by DEPC essentially as described previously (13). After 10 and 60 min of reaction aliquots were removed and the reaction stopped by precipitation with 4 volumes of cold ethanol and 10 μl of 100 μg/ml calf thymus DNA. Pellets were dissolved in 1 M piperidine and heated to 95°C for 15 min. Samples were then evaporated to dryness, dissolved in formamide, and loaded on a 15% polyacrylamide sequence gel. Exposure and quantitition were carried out with with an SF Phosphorimager from Molecular Dynamics (Sunnyvale, CA) using the Image Quant software.

Spectroscopy

Ultraviolet absorption spectra were obtained as described previously (22) using a Uvikon 820 spectrophotometer equipped with computer-controlled thermostated cuvette holders and data acquisition. Heating cycles were measured from 4°C to 90°C at intervals of ~4°C incremented every 6 min. Thermal transitions, recorded at a single wavelength were measured at intervals of 1°C. Cuvette path lengths were 1 cm for denaturation curves and 1 mm for absorption and CD spectra. Hyperchromicity data were corrected and analyzed as described previously (26) Single wavelength melting data were analyzed by 6 parameter fitting functions described below. CD measurements were made from 195 to 320 nm at 10°C and 70°C on a Jasco-720 CD spectrometer. Scanning was carried out with 1 nm bandwidth and a 0.2 nm spectral resolution. The buffer was 10 mM $MgCl_2$, 10 mM $NaPO_4$, pH 7.0. CD and UV absorption spectra were analyzed and plotted with KaleidaGraph.

Analysis of helix–coil transitions

The helix–coil transitions were fit to a concerted two-state model (26,38,39) or to a zipper multistate model based on a statistical mechanical description for duplex states with varying degrees of hydrogen-bonding (40) The latter formalism was required for the longer 30-mer ps-L1·L2 duplex (Fig. 1).

Model 1. Two-state (all-or-none) mechanism

The temperature and concentration dependent equilibrium constant, K, for a concerted helix (duplex)→coil transition is given by

$$K_c = \frac{\theta_c^2}{1-\theta_c}\gamma C_t \qquad (1)$$

where θ_c is the fraction of strands in the coil form (0.5 at the T_m), C_t is the total strand concentration, and the coefficient γ equals 0.5 for a heterodimer and 2 for a homodimer. The van't Hoff transition enthalpy, ΔH_{vH}, is defined as

$$\Delta H_{vH} = -R\frac{\partial \ln K_c}{\partial T^{-1}} \quad (2)$$

where R is the gas constant and T is the absolute temperature. The thermodynamic parameters are obtained from a direct fit of the absorbance vs. temperature profile, $A^{\lambda,T}$, generally at the wavelength λ of 258 nm. The fit parameters are: ΔH_{vH}, T_m, and the intercepts and relative slopes b_h^λ, m_h^λ) of the 'lower' (low temperature, double-stranded helical form) and (b_c^λ, m_c^λ) of the 'upper' (high temperature, single-stranded coil form) baselines. From Eqs 1 and 2,

$$A^{\lambda,T} = A_h^{\lambda,T} + (A_c^{\lambda,T} - A_h^{\lambda,T})\theta_c \quad (3)$$

$$A_h^{\lambda,T} = b_h^\lambda (1 + m_h^\lambda T^{\circ C}) \quad (3a)$$

$$A_c^{\lambda,T} = b_c^\lambda (1 + m_c^\lambda T^{\circ C}) \quad (3b)$$

$$\theta_c = \frac{\sqrt{1+8E_T} - 1}{4E_T} \quad (3c)$$

$$E_T = \frac{K_{T_m}}{K_T} = exp\left[(\Delta H_{vH}/R)(T^{-1} - T_m^{-1})\right] \quad (3d)$$

where $A_h^{\lambda T}$, and $A_c^{\lambda T}$ represent the absorbances of the pure helical and coil forms, respectively. By defining the linear parameters on the Celsius temperature scale (Eqs 3a,b) good initial estimates of b_h^λ and b_c^λ are obtained by inspection. It is also our experience that faster convergence and more physically realistic values are achieved with the given form of Eq. 3 than with numerous alternative expressions. The factors representing the temperature dependence of absorbance, m_h^λ and m_c^λ, are specific for a given DNA type and solution condition but defined so as to be concentration independent. Equation 3 assumes a linear dependence on temperature of the extinction coefficients, $\epsilon_h^{\lambda T}$ and $\epsilon_c^{\lambda T}$, of the helical and coil species (41); thus, the terms b_h^λ and b_c^λ represent the products of $\epsilon^{\lambda,T}$, optical path length, and concentration. By avoiding explicit reference to the transition entropy ΔS in Eq. 3d, both the homodimer and heterodimer cases can be accommodated, in contrast to other formulations (39,42). The data from the 3-D melting profiles were also analyzed with a global fitting program in which Eq. 3 is evaluated at multiple wavelengths assuming a common function E_T (Eq. 3d; 26).

Model 2. Multistate zipper mechanism

The system is considered to consist of the separated strands of chain length N in equilibrium with duplex species in perfect alignment but with a statistically positioned contiguous hydrogen-bonded segment of variable length (40). The corresponding system partition function q corresponds to the sum of the individual equilibrium constants, K_j, for the formation of the j-bonded duplex species; $j = 1-N$. Thus,

$$q = \sum_{j=1}^{N} K_j = \kappa \sum_{j=1}^{N} (N - j + 1)s^{j-1} \quad (4)$$

where $\varkappa$ is the equilibrium constant for formation of the first base pair and is generally regarded as temperature independent (43). We maintain this assumption in the treatement below, although initiation enthalpies can be incorporated easily. Values of $\varkappa$ from the literature vary from 10^{-5} to 10^{-2} M^{-1}; we used 4×10^{-3} M^{-1} (44). The quantity s is the equilibrium constant for formation of successive base pairs in the chain propagation phase of duplex formation. It is defined thermodynamically in Eq. 5 in terms of the unit enthlapy and entropy changes, Δh_{vH} and Δs, for the reverse reaction, i.e. disruption of the base pair. This usage maintains consistency with Model 1 and our prior treatment of oligonucleotide helix−coil transitions.

$$s = exp\left(\frac{\Delta h_{vH}/T - \Delta s}{R}\right). \quad (5)$$

The coefficient in Eq. 4 accounts for the statistical weights of the various species constituting the j-bonded duplex. The summation can be expressed in a closed form.

$$q = \kappa \cdot \frac{s^{N+1} - (N+1)s + N}{(s-1)^2} \quad (6)$$

From Eq. 1, the fraction of strands in the coil form is a function of q and C_t.

$$\theta_c = \frac{\sqrt{1 + 4q \cdot \gamma C_t} - 1}{2q \cdot \gamma C_t} \quad (7)$$

Finally, we require the mean fraction of paired bases in the population of duplex species $\langle j/N \rangle$. This quantity is derived as the weighted sum of the individual probabilities and lies in the range 1 to N^{-1}.

$$\langle j/N \rangle = \frac{\kappa}{q}\sum_{j=1}^{N} j \cdot K_j = 1 - \frac{2s^{N+1} - (Ns - N + 1)(Ns - N + s)}{N(s-1)[s^{N+1} - (N+1)s + N]} \quad (8)$$

Invoking the standard assumption that an unpaired base in the duplex and coil forms absorbs equally, Eqs 7 and 8 lead to an expression for the melting profile analogous to Eq. 3.

$$A^{\lambda,T} = A_c^{\lambda,T} + (A_h^{\lambda,T} - A_c^{\lambda,T})(1 - \theta_c) \cdot \langle j/N \rangle \quad (9)$$

Fitting data to models 1 and 2

Macros for fitting data according to Eqs 3 and 9 (*helix_9_fit* and *helix_10_fit*, respectively) were developed for the program KaleidaGraph (v. 2.1.4; Abelbeck Software). Equation 5 was cast in terms of a T_m corresponding to the fully paired duplex species ($j/N = 1$) and a total strand concentration C_t. From Eqs 1, 4, and 5,

$$\Delta s = \left[\frac{\Delta h_{vH}}{T_m} - \frac{R}{N-1} ln(2/\kappa\gamma C_t) \right] \quad (10)$$

$$s = exp\left[\frac{\Delta h_{vH}}{R}(T^{-1} - T_m^{-1}) + \frac{ln(2/\kappa\gamma C_t)}{N-1} \right] \quad (11)$$

The measured melting temperatures from both methods of analysis were corrected to standard strand concentrations, C_r, of 10^{-6} M (heterodimers) and 0.5×10^{-6} M (homodimers); the difference compensates for the favorable statistical bias in the recombination of identical strands.

$$T_{m,s}^{-1} = T_{m(easured)}^{-1} + (R/\Delta H_{vH}) ln(C_t/C_r) \quad (12)$$

For the purposes of comparing analyses from Models 1 and 2, $\Delta S°$ and $\Delta G_T°$ values were calculated for the fully paired duplex species from the values of ΔH_{vH} (obtained directly in Model 1 or from Δh_{vH} in Model 2, Eq. 13) and $T_{m,s}$.

$$\Delta H_{vH} = (N-1)\Delta h_{vH} \quad (13)$$

$$\Delta S° = \Delta H_{vH}/T_{m,s} - R ln(2/\gamma C_r) \quad (14)$$

$$\Delta G_T^{o} = \Delta H_{vH} - T\Delta S° \quad (15)$$

DNA specific spectroscopic parameters were also computed: *hyp*(%), the relative absorption hyperchromism in passing from the fully helical to the fully coil form, evaluated at T_m; and $\partial\, ln\, A/\partial T$, the fractional change in the absorbances of the helical and coil forms per degree increase in temperature, evaluated at T_m.

$$hyp(\%) = 100\left[\frac{b_c^{\lambda}(1+m_c^{\lambda}T_m^{°C})}{b_h^{\lambda}(1+m_h^{\lambda}T_m^{°C})} - 1 \right] \quad (16)$$

$$\partial ln A_h/\partial T|_{T_m} = (m_h^{\lambda-1} + T_m^{°C})^{-1} \quad (17)$$

$$\partial ln A_c/\partial T|_{T_m} = (m_c^{\lambda-1} + T_m^{°C})^{-1} \quad (18)$$

RESULTS

Electrophoretic properties

The formation of the 30 bp ps-L1·L2 (Fig. 1) and the component 15 bp ps-F5·F6 and ps-GA_{15} duplexes were characterized by native gel electrophoresis. Radioactively labeled DNA was incubated alone or with a two-fold excess of complementary unlabeled strand at 80°C before slow cooling to 4°C and loading onto a native polyacrylamide gel containing 10 mM $MgCl_2$ and operated at 7°C. The results are shown in Fig. 2. In panel A

```
GA15          5'-GAGAGAGAGAGAGAG
GA15          5'-GAGAGAGAGAGAGAG

F5            5'-TTTTTATTAAATATA
F6            5'-AAAAATAATTTATAT

L1      5'-GAGAGAGAGAGAGAGTTTTTATTAAATATA
L2      5'-GAGAGAGAGAGAGAGAAAAATAATTTATAT
           1    5    10   15   20   25   30

F5            5'-TTTTTATTAAATATA
F7            3'-AAAAATAATTTATAT

L1      5'-GAGAGAGAGAGAGAGTTTTTATTAAATATA
L3      3'-CTCTCTCTCTCTCTCAAAAATAATTTATAT
```

Figure 1. Oligonucleotide duplexes and abbreviations used in this study. GA_{15} and F5+F6 have been shown to form parallel-stranded duplexes (ps-GA_{15} and ps-F5·F6) (9,11,13). L1+L2 forms a ps duplex (ps-L1·L2, this study). F5+F7 and L1+L3 form anti-parallel duplexes (aps-F5·F7, aps-L1·L3). F5, F6, and F7 were designated as F1, F2, and F3, respectively, in previous studies (9).

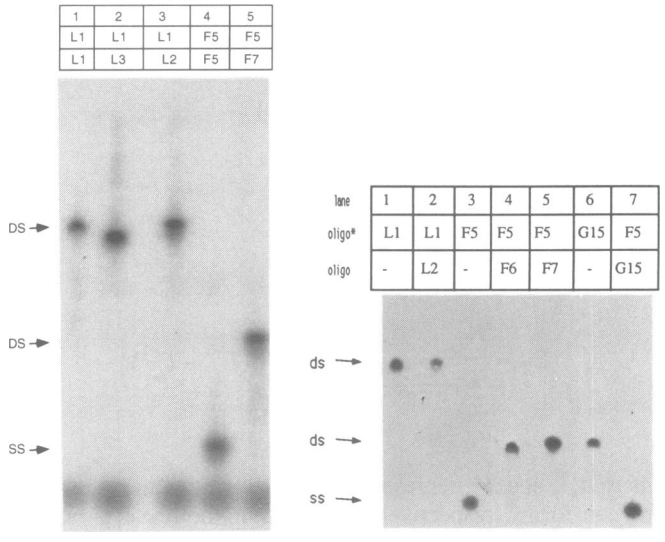

Figure 2. Native gel electrophoresis of ps and aps duplexes. DNA migrating as a duplex is marked as DS, and single-stranded species as SS. **(Right panel)** Lanes: (1) L1 alone; (2) L1 plus L2; (3) F5 alone; (4, 5, 7) F5 plus F6, F7, and GA_{15}, respectively; (6) GA_{15} alone. **(Left panel)** Native gel electrophoresis of L1 as a self-complex (lane 1) and with aps and ps complements (lanes 2 and 3, respectively) Single-stranded F5 alone (lane 4) and duplex aps-F5·F7 (lane 5) are shown as mobility references. Oligonucleotides in the upper row in the legend indicate the strand that was radioactively labeled. The concentration of the labeled strand concentration was 1 μM and of the unlabeled strand 2 μM. Gels contained 15% polyacrylamide and 10 mM $MgCl_2$, and were run at 7°C.

it is seen that L1 formed a stable duplex both with itself and its parallel-oriented complement L2 (lanes 1 and 2). The homoduplex of L1 was presumably mediated through the $d(GA)_7G$ portion of the oligonucleotide, as in the case of the ps-GA_{15} reference (lane 6). F5 formed a stable duplex with its parallel (F6) or anti-parallel (F7) complement but neither with itself nor with GA_{15} (lanes 3, 4, 5, and 7). It is seen that the ps_{RY} duplex migrated somewhat faster than the reference aps molecule. The greater electrophoretic mobility of ps- relative to aps-DNA is a consistent finding (17–19,22). The GA_{15} oligonucleotide formed a ps_{RR} homoduplex (ps-GA_{15}) (lane 6), with a mobility similar to that of ps-F5·F6 (lane 4), as reported previously (13). Figure 2B shows the relative mobility of the ps-L1·L2 and the L1

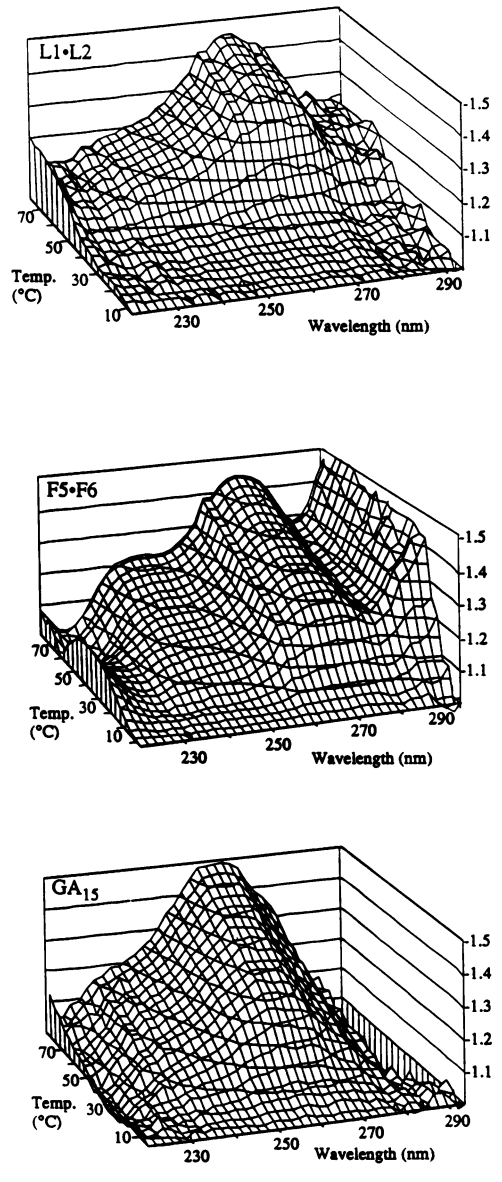

Figure 3. Thermally resolved UV absorption spectra of ps-L1·L2 and component 15-mer duplexes. The data are expressed as the ratio of $A^{\lambda,T}/A^{\lambda,T_0}$ where T_0 is the initial temperature. All experiments were in 10 mM $MgCl_2$, 10 mM Na-cacodylate, pH 7.0. The small spike at 260 nm is an artifact. Top, ps-L1·L2; middle, ps-F5·F6; bottom, ps-GA_{15}. Concentrations were 0.72 μM, 3.2 μM and 1.7 μM, respectively.

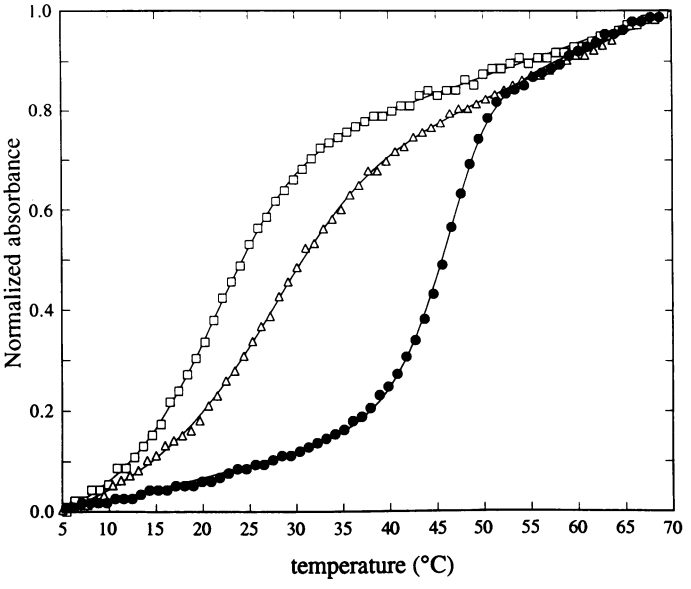

Figure 4. Normalized thermal helix−coil transitions and fits at 258 nm for ps-L1·L2 (−−●−−), ps-F5·F6 (−−□−−), and ps-GA_{15} (−−Δ−−). Data were fitted to Models 2 (ps-L1·L2) and 1 (ps-F5·F6 and ps-GA_{15}). Absorbances were normalized by subtracting the values at 5°C and dividing by the difference absorbance ($A^{70°} - A^{5°}$). Concentrations were 1.3 μM, 2.0 μM and 2.2 μM, respectively.

homodimer relative to aps-L1·L3 (Fig. 1). It can be seen that the ps complexes (lanes 1, 3) exhibited about the same mobility as the 30 bp aps duplex L1·L3 (lane 2), although the latter migrated slightly faster, probably due to the overall lower molecular weight of this duplex. Lanes 4 and 5 contained single stranded F5 and aps duplex F5·F7 respectively as relative mobility markers. In these and other electrophoretic experiments, no radioactivity was detected in the loading wells, indicating that aggregation of the oligonucleotides did not occur. Only single-stranded and duplex species were observed. Tetraplexes or other higher order species that might have been expected to migrate as slower moving bands on a native gel were not evident.

Helix−coil transitions

It has been shown in earlier studies that different strand orientations result in distinctive patterns of hyperchromicity as a function of wavelength (9,26). These features presumably reflect overall differences in helical geometry, particularly base stacking, that are not readily apparent from a single low temperature absorption spectrum. In order to compare the stereochemistry of ps-L1·L2 to that of the constituent half molecules, we measured the hyperchromicity patterns of all three DNA duplexes as a function of temperature. The surface plots of hyperchromicity (Fig. 3) were generated by dividing the spectra of the DNA at increasing temperatures by the spectra of native duplexes at 4°C. All three duplexes showed the pattern specific for ps-DNA, characterized by a peak at 265 nm and weak shoulder at 240 nm, in contrast to the plateau at 240−260 nm distinctive for aps-DNA (26).

Ultraviolet melting curves provided the means for comparing the overall stability of the ps-L1·L2 to the component 15-mer duplexes, ps-F5·F6 and ps-GA_{15} (Fig. 4). All three exhibited cooperative, fully reversible helix−coil transitions from which melting temperatures (T_m) and the transition enthalpies and entropies corrected to standard reference strand concentrations could be extracted (Table I). The individual 15-mers had similar melting temperatures: 21°C for ps-F5·F6 and 22°C for ps-GA_{15}. The validity of the two-state transition mechanism (Model 1) for the separate sequence motifs (left and right halves of ps-L1·L2) was determined previously by direct calorimetric measurement of ps_{RY} (29) and a linear fit of T_m^{-1} vs. $ln\ C_t$ for ps_{RR} (13). Furthermore, evaluation of the melting curves of the separate 15-mers according to Model 2 yielded equivalent estimates of the thermodynamic parameters.

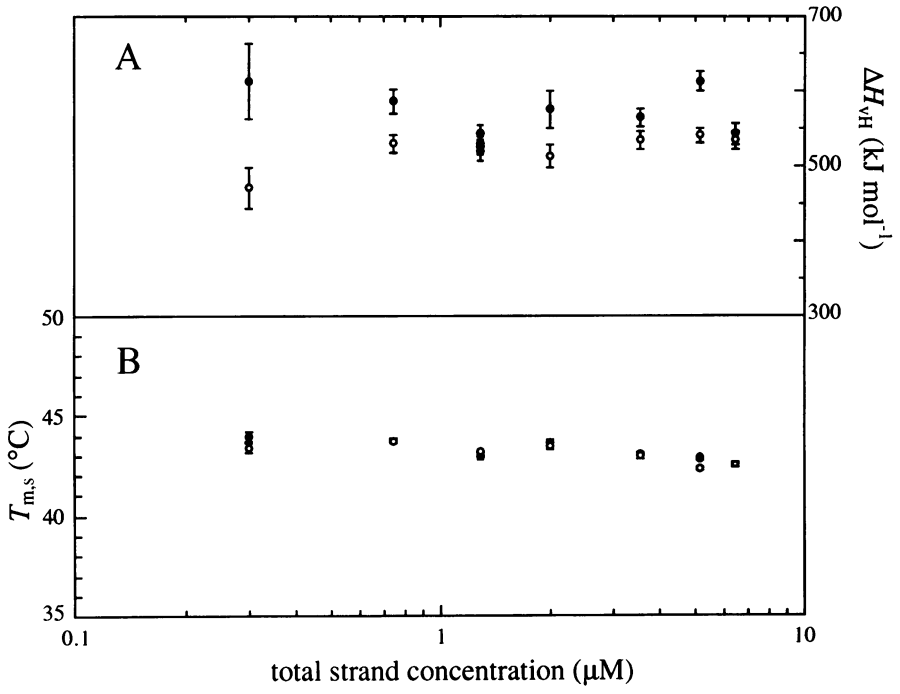

Figure 5. Determination of ΔH_{vH} (**A**) and $T_{m,s}$ (**B**) for ps-L1·L2 according to the statistical mechanical formalism (Model 2) from measurements at different total strand concentration. The indicated values correspond to Eqs 12 and 13 and thus refer to a constant reference strand concentration (1 μM). Analyses from ascending (●) and descending (○) limbs of the thermal transition curves. The indicated errors are standard deviations from the individual fits. In several instances, $T_{m,s}$ points are coincident. All solutions contained 10 mM $MgCl_2$, 10 mM Na-cacodylate, pH 7.0.

Table I. Thermodynamic parameters for helix–coil transition of ps-DNA duplexes[a]

Duplex	Chain length N	$T_{m,s}$[b] (°C)	ΔH_{vH} (kJ mol^{-1})	Δh_{vH}[c] (kJ mol^{-1} nn^{-1})	$\Delta S°$[d] (kJ mol^{-1} K^{-1})	$\Delta G°_{37°}$[e] (kJ mol^{-1})	$\Delta g°_{37°}$[f] (kJ mol^{-1} bp^{-1})	hyp[g] (%)	$\partial A/\partial T$[h] (h, c) (10^3·K^{-1})
ps-F5·F6	15	21.1 ± 1.6	315 ± 31	22.5 ± 2.2	0.78 ± 0.12	25.8 ± 1.5	1.72 ± 0.10	20 ± 6	1.4, 1.8
ps-GA_{15}	15	21.8 ± 0.1	236 ± 34	16.9 ± 2.4	0.73 ± 0.17	24.3 ± 2.2	1.62 ± 0.15	15 ± 2	2.1, 2.9
sum			551 ± 46			50.1 ± 2.7			
mean				18.7 ± 2.3			1.67 ± 0.18	18 ± 8	1.8, 2.3
ps-L1·L2	30	43.1 ± 0.5	569 ± 33	19.6 ± 1.1	1.67 ± 0.10	49.8 ± 1.3	1.66 ± 0.04	19 ± 2	1.6, 2.1

[a]Measurements in 10 mM $MgCl_2$, 10 mM Na-cacodylate, pH 7.0. The data for ps-F5·F6 and ps-GA_{15} were analyzed according to Model 1 (single and multi wavelength analysis). The data for ps-L1·L2 were analyzed according to Model 2 for both the ascending and descending limbs of the temperature profile (Fig. 5). The values of ΔH_{vH} from the descending limb were systematically lower (~7%) and are not included. The indicated errors are standard deviations calculated with data from different experiments.
[b]Melting temperature corrected to a standard total strand concentration, C_r, of 1 μM (heterodimers) and 0.5 μM (homodimers) according to Eq. 12. All determinations were at $A^{260} \approx 0.3$ in 1 or 0.3 cm pathlength cells except for the concentration range used for ps-L1·L2 in Fig. 5 ($A^{260} \approx 0.04-0.6$).
[c]ΔH_{vH} per nearest neighbor interaction (nn).
[d]ΔS calculated for standard strand concentration C_r.
[e]ΔG calculated for 37°C and standard strand concentration C_r.
[f]$\Delta G_{37°}$ per base pair (bp).
[g]Absorption hyperchromicity at 258 nm (260 nm for ps-GA_{15}) according to Eq. 16. Calculated with the fit parameters from Models 1 and 2.
[h]Temperature dependence of A^{258} (A^{260} for ps-GA_{15}) according to Eqs 17 (helix) and 18 (coil). Values varied from those indicated by ±30%.

In contrast, the thermal transition data of ps-L1·L2 analyzed by the two models yielded different results. The estimations of apparent ΔH_{vH} derived with the all-or-none formalism (Model 1) were ~10% lower than those according to the more appropriate zipper mechanism (Model 2). Furthermore, the alternative approach provided by Model 1 to the evaluation of ΔH_{vH} based on the regression T_m^{-1} vs. $ln\ C_t$ led to unrealistically high, statistically unreliable values. Model 2, however, yielded constant values of ΔH_{vH} over a range of strand concentrations (Fig. 5, Eq 12). The mean ΔH_{vH} of 569 kJ mol^{-1} was substantially higher than for the individual half molecules (Table I). In addition, a constant $T_{m,s}$ of 43°C was obtained for ps-L1·L2 (Fig. 5), a value substantially higher that the 21–22°C for the half molecules. A simulation computed with the fit parameters for $C_t = 5.2$ μM indicated that at the calculated $T_{m,s} = 1.93$, $<j/N> = 0.93$, and $\theta_c = 0.29$, corresponding to 7% fraying and 29% duplex at the apparent transition midpoint.

The comparison of thermodynamic characteristics of the different DNAs was facilitated by examination of the reduced parameters, i.e. enthalpy change per nearest-neighbor interaction

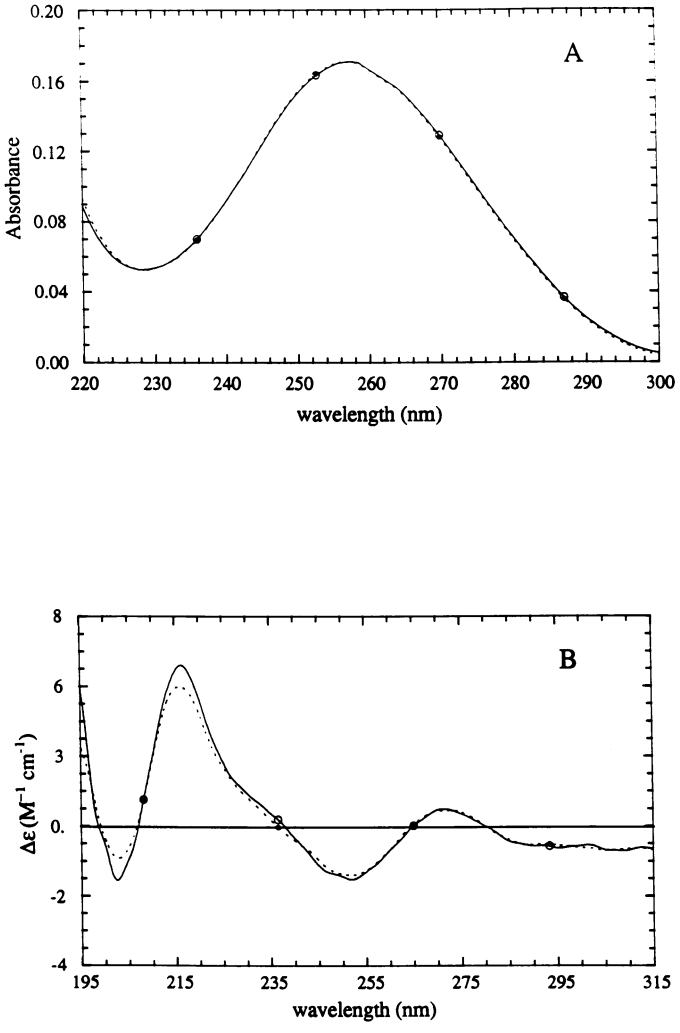

Figure 6. Spectra of denatured single-stranded species. Ultraviolet absorption (**A**) and CD (**B**) spectra of ps-L1·L2 (---●---) and the linear sum of spectra of ps-F5·F6 and ps-GA_{15} (– – ○ – –) at 70°C in 10 mM $MgCl_2$, 10 mM Na-phosphate, pH 7.0. DNA concentration, 0.52 μM

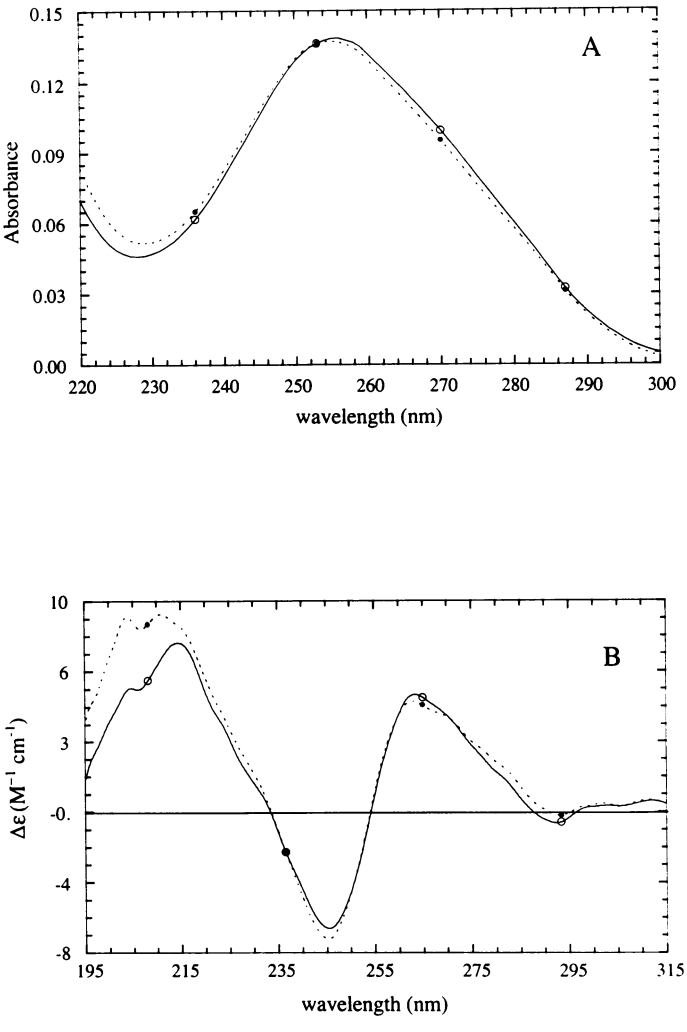

Figure 7. Spectra of the native double helical forms. Ultraviolet absorption (**A**) and CD (**B**) spectra of ps-L1·L2 (---●---) and the linear sum of spectra of ps-F5·F6 and ps-GA_{15} (– – ○ – –) at 10°C in 10 mM $MgCl_2$, 10 mM Na-phosphate, pH 7.0. Same concentration as in Fig. 6.

and free energy change per base pair (Table I). In this manner one compensates for the different lengths of the molecules being compared, so as to focus on the individual base pair properties. This approach also accomodates the presumed additional stacking interaction in ps-L1·L2 generated by the fusion of the ps-GA_{15} and ps-F5·F6 duplexes. The Δh_{vH} of the ps-F5·F6 duplex composed entirely of d(A·T) base pairs was somewhat higher than for the 15 bp ps-GA_{15} duplex consisting of d(G·G) and d(A·A) base pairs (22 kJ mol^{-1} nn^{-1} vs. 17 kJ mol^{-1} nn^{-1}). The mean of these values is in excellent agreement with the Δh_{vH} of 20 kJ mol^{-1} determined for the ps-L1·L2 duplex. Based on $\Delta g^{\circ}_{37^{\circ}}$, the normalized free energy change per base pair for the helix→coil transition at 37°C, all three DNAs were comparable in stability; the values were 1.72, 1.62, and 1.66 kJ mol^{-1} bp^{-1} for ps-F5·F6, ps-GA_{15}, and ps-L1·L2, respectively (Table I).

In addition to the additional stacking interaction, there are other potential differences in the thermodynamic descriptions of the 30-mer and the individual 15-mer duplexes. Ps-L1·L2 has two non-identical ends (and, if disordered, the central junction) from which denaturation can initiate, compared to the individual 15-mers each with two equivalent ends and uniform composition. In terms of the nucleation/chain propagation model involving a negligible enthalpy change associated with the formation/breakage of the first/last base pair, one can incorporate in $\Delta h^{junct}_{L1\cdot L2}$ the difference between the ΔH_{vH} of ps-L1·L2 and the combined values of its constituent halves, all potential contributions arising from the central sequence junction (step $|G\text{-}G|_{15} \Rightarrow |T\text{-}A|_{16}$, Fig. 1). From Table I, $\Delta h^{junct}_{L1\cdot L2} \approx 18$ kJ mol^{-1}, a positive value that would be consistent with an additional, stabilizing stacking interaction. However, the statistical uncertainty (formally ± 57 kJ mol^{-1} from the combination of the individual standard deviations) renders the interpretation tentative.

Denaturation curves of oligonucleotides L1 and L2 alone were also measured in order to support the presumption that L1 and L2 migrate as duplexes on native polyacrylamide gels because of parallel-stranded interactions between the GA_{15} segments of the two strands. The melting of the self-structure formed by each

oligonucleotide was examined in 10 mM $MgCl_2$. L1 and L2 both underwent weakly cooperative transitions at 24°C and 28°C, respectively, close to the T_m of ps-GA_{15}. The different melting temperatures may reflect an additional but differential stabilization from self-complementation between the AT portions of the two strands. Neither F5 nor F6 alone formed homoduplexes under the same conditions, providing further evidence that the GA_{15} segment was responsible for the secondary structure of L1 and L2 individually.

UV absorption and circular dichroism spectroscopy

The correspondence of the ps-L1·L2 conformation with those of the component halves was explored further by UV absorption and CD spectroscopy. The CD and UV spectra of all species were measured at 10°C and 70°C in 10 mM $MgCl_2$. We assumed that the UV absorption spectrum of denatured ps-L1·L2 should be matched closely by the sum of the spectra of equimolar denatured ps-F5·F6 and ps-GA_{15} under the same conditions (70°C, 10 mM $MgCl_2$); differences in the contributions of terminally located bases were deemed to be negligible. Thus,

$$\varepsilon_{L1+L2}^{\lambda,70^\circ} = \frac{\varepsilon_{GA_{15}}^{\lambda,70^\circ} + \varepsilon_{F5+F6}^{\lambda,70^\circ}}{2} \qquad (19)$$

The scaling factors (x, y) required to generate a linear combination of reference absorption spectra of the two 15-mers matching the spectrum of ps-L1·L2 at 70°C were computed with the fitting program KaleidaGraph according to

$$A_{L1+L2}^{\lambda,70^\circ} = x \cdot A_{F5+F6}^{\lambda,70^\circ} + y \cdot A_{GA_{15}}^{\lambda,70^\circ} \qquad (20)$$

The absolute values of the coefficients x and y depend on the concentrations at which the reference spectra are taken. Their ratio x/y, however, is uniquely related to that of the extinction coefficients of the component 15-mers in Eqs 3 and 9, inasmuch as the half molecules were necessarily represented stoichiometrically in the 30-mer duplex. From Beer's Law, the ratio of the extinction coefficients of GA_{15} and of the combination (F5 + F6) is given accurately at any temperature by

$$\Phi^{\lambda,T} = \frac{\varepsilon_{F5+F6}^{\lambda,T}}{\varepsilon_{GA_{15}}^{\lambda,T}} = (x/y) \cdot \frac{A_{F5+F6}^{\lambda,T}}{A_{GA_{15}}^{\lambda,T}} \qquad (21)$$

The fit to Eq. 20 was excellent throughout the spectral range (Fig. 6A) and yielded $\Phi^{260,70^\circ} = 0.95$. From these relationships it was possible to obtain the extinction coefficients of the various duplexes (Eq. 7) formed by mixing calibrated stock solutions of the individual strands and using as the primary reference the most accurate extinction coefficient available in the literature for any one of the components. For example, the reported value for single-stranded $d(GA)_n$ at 260 nm is 9.5 mM base^{-1} cm^{-1} at 21°C (45). Extrapolating to 70°C using the upper baseline of a ps-GA_{15} denaturation (Eq. 3), we calculated an $\epsilon^{260,70^\circ}$ of 10.9 mM base^{-1} cm^{-1}. With the value of Φ cited above, an $\epsilon^{260,70^\circ}$ for (F5 + F6) of 10.3 mM base^{-1} cm^{-1} was obtained, in good agreement with the value 10.6 mM base^{-1} cm^{-1} at 80°C

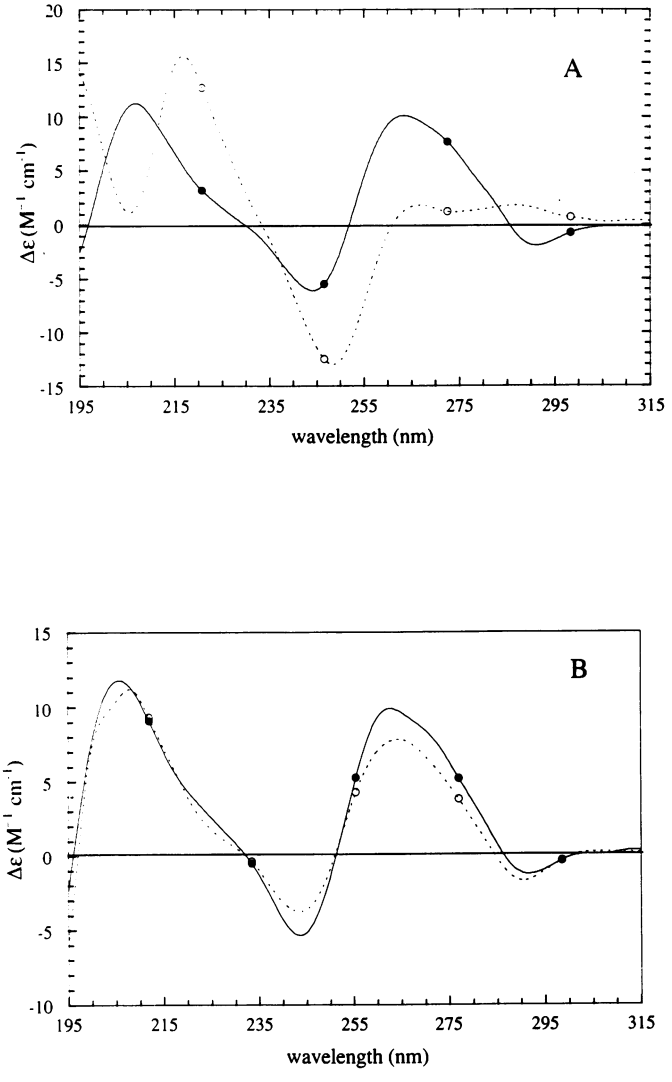

Figure 8. Circular dichroism spectra of ps-F5—F6 (A) and ps-GA_{15} (A, B). (**A**) ps-F5·F6 (---○---) and ps-GA_{15} (– – ● – –) in 10°C, 10 mM $MgCl_2$, 10 mM Na-cacodylate, pH 7.0. Concentrations 0.94 μM and 1.3 μM, respectively. (**B**) ps-GA_{15} at 5°C in 100 mM NaCl, 10 mM K-phosphate, pH 7.0 (---○---) and 10 mM $MgCl_2$, 10 mM K-phosphate, pH 7.0 (– – ● – –).

calculated by standard algorithms for a similar 25 bp ps duplex (ps-D1·D2) containing only adenine and thymine (29).

The scaling factors and extinction coefficients from the above analysis were used to generate theoretical UV absorption and CD spectra of ps-L1·L2 at 10°C and 70°C as the appropriately weighted sum of the spectra of the half molecules (Eq. 8). The agreement between the calculated and experimental high temperature CD spectra of ps-L1·L2 was quite good (Fig. 6B), although the experimental spectrum had somewhat stronger positive and negative lobes at 215 and 200 nm, respectively. A similar comparison was carried out at 10°C, a temperature at which all the duplexes should have been fully formed (Fig. 7A, B). The experimental and calculated UV absorption spectra of ps-L1·L2 (Fig. 7A) exhibited similar levels of hypochromism and only a 1 nm blue shift in the spectrum of ps-L1·L2 relative to the combined spectrum of ps-F5·F6 and ps-GA_{15}. The

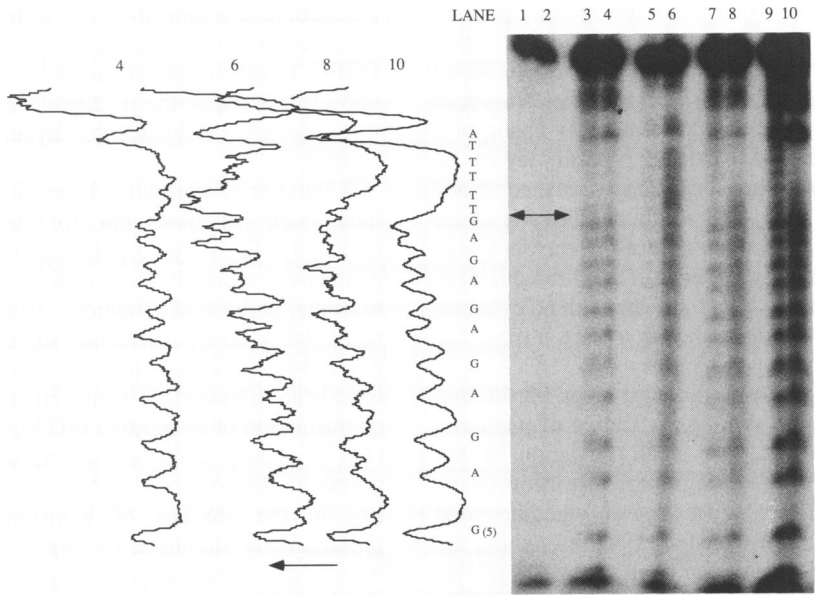

Figure 9. DEPC modification of ps L1·L2 and aps L1·L3. Lanes 1,2, piperidine reaction of L1 and L2, respectively, without prior reaction with DEPC. Lanes 3–10, DEPC modification. Odd and even numbered lanes represent aliquots after 10 and 60 min of reaction, respectively. Lanes 3,4, ps-L1·L2 with the L1 strand radiaoctively labeled. Lanes 5,6, ps-L1·L2 with L2 labeled. Lanes 7,8, aps-L1·L3 with L1 labeled. Lanes 9,10, labeled L1 alone in the single-stranded form. To the left are line graphs of the relative radioactivity of the indicated lanes, The data were acquired and evaluated with an SF Phosphorimager (Molecular Dynamics).

corresponding CD spectra (Fig. 7B) also showed good agreement. All the peak positions and the crossover points at 231 and 255 nm remained essentially unchanged, while only a 2 nm upshift was observed at the 285 crossover point. In the lower wavelength region, however, some deviations between the experimental and calculated spectra were evident. Below 215 nm, the circular dichroism corresponding to the sum of ps-F5·F6 and ps-GA_{15} was less than that measured for ps-L1·L2. The spectra of the individual 15-mers (Fig. 8A) indicated that the signal in the 200–215 nm region was due mainly to ps-GA_{15}. To investigate the source of these discrepancies, we compared the spectra of ps-GA_{15} in NaCl (100 mM) and $MgCl_2$ (10 mM) (Fig. 8B). The NaCl spectra showed differences in intensity at all four lobes as well as small changes in peak positions and the crossover point above 275 nm. The CD spectrum of ps-GA_{15} in $MgCl_2$, however, led to a better fit of the ps-L1·L2 data in combination with the spectrum of ps-F5·F6, as compared to the results of an analysis using the CD measurements in NaCl. Further spectroscopic studies are being undertaken in order to characterize these apparent conformational differences of ps-GA_{15} in Na^+ or Mg^{2+}.

A final test for the concordance between the spectral properties of the 15-mer DNAs and ps-L1·L2 was provided by a comparison of the helix→coil hyperchromicities and temperature dependent absorption properties (Table I). The computed hyperchromicity at 258 nm of the 30-mer (19±2%) was compatible with the values for the half molecules (20 ± 6% and 1 ± 3%). Likewise, the temperature coefficients for the helix and coil absorbances (Eqs. 17 and 18) were consistent (coil > helix, values for ps-L1·L2 intermediate between those for ps-F5·F6 and ps-GA_{15}).

Chemical modification with diethylpyrocarbonate (DEPC) was performed in order to determine if distortions at the conformational junction in ps-L1·L2 disrupted base pairing or stacking in that region. DEPC, which carboxylates purines at the N-7 position, reacts strongly with single-stranded and only weakly with double-stranded DNA. Klysik and co-workers (27) have shown that parallel-stranded DNA containing A-T base pairs shows only a weak reactivity, similar to anti-parallel B-form DNA. Additionally, d(GA) oligonucleotides also show a marked decrease in reactivity in passing from the single-stranded to the double-stranded ps form (13). The reactivities of ps-L1·L2, aps-L1·L3, and single-stranded L1 are compared in Fig. 9. Both the ps and aps species (lanes 3–9) showed a similar reactivity that was considerably less than that of the single-stranded L1 control (lanes 9,10). L1 was reacted without Mg^{2+} so as to suppress secondary structure in the GA segment of this oligonucleotide. These results are consistent with the previously reported reactivity of the two ps conformations probed separately. The plotted lane tracings also confirm the absence of hyperreactivity at the junction between the ps-GA and ps-AT regions. This feature is best perceived by comparing the tracings from lane 4 (ps) and lane 8 (aps) in which L1 is the radioactively labeled species in both duplexes. We conclude that there was no significant distortion of the helical structure(s) at the sequence junction.

DISCUSSION

This study has established that the two 30 nucleotide long sequences L1 and L2 form a ps duplex that is equivalent thermodynamically and spectroscopically to the sum of the individual, constituent ps motifs (ps-GA_{15} and ps-F5·F6) characterized previously (9,11,13), and representing distinct subclasses in the family of ps-DNA conformations. ps-L1·L2 is stable at physiological pH and salt conditions. In native gel electrophoresis, only a single band with a mobility comparable to that of the aps equivalent is observed. There is no evidence for higher order aggregates or hairpin structures.

The CD and UV absorption spectra at low temperature provide a means to probe for structural adjustments in ps-L1·L2 resulting from the juxtaposition of the two ps motifs. There is good agreement between the spectra of ps-L1·L2 and of the component half molecules. The experimental and calculated UV absorption spectra of ps-L1·L2 (Fig. 6A) exhibit similar levels of hypochromism and only a 1 nm blue shift relative to the combined spectra of ps-F5·F6 and ps-GA_{15}. Thus, the degree of stacking in ps-L1·L2 remains essentially the same as in the separated halves. The 3-D hyperchromicity patterns of all three duplexes show the characteristic ps peak at about 265 nm with no evidence of the aps duplex pattern, a double peak with a plateau from 230 to 270 nm (26).

The CD spectra of ps-L1·L2 and the sum of ps-F5·F6 and ps-GA_{15} at 10°C are also quite similar, indicative of unaltered stacking interactions. However, the small deviation in the 200–220 nm region may reflect a degree of distortion in the ps-GA_{15} segment of ps-L1·L2. To assess whether such distortions might result from a propagated effect throughout the GA portion of the helix and originating from the AT segment, we compared the spectra of ps-GA_{15} in NaCl and $MgCl_2$ (Fig. 7B). The decomposition of the CD spectra of ps-L1·L2 was most accurate when using the reference spectrum of ps-GA_{15} in Mg^{2+} rather than in Na^+. The preferential stabilization of ps-GA_{15} by Mg^{2+} (13) suggests that divalent cations generate a somewhat different conformation than that adopted in Na^+, and that this structure prevails in the 30 bp long duplex. The positive dichroism of the 210 nm band decreases upon thermal denaturation under both salt conditions. Thus, the higher amplitude of the 210 nm band in the spectrum of ps-L1·L2 may reflect an increased stabilization of the $d(GA)_n$ half of the molecule under the influence of the ps_{RY} region. For example, the end regions may be less susceptible to fraying in the composite molecule. However, we would stress the similarities rather than the deviations in the spectral fitting, inasmuch as they confirm the anticipated secondary structure, particularly in the ps-GA_{15} segment. That is, in order for the purine–pyrimidine half to be in register, the purine–purine segment must feature the d(G·G) and d(A·A) base pairs proposed previously (13). Any other arrangement would result in one or more looped out bases at the junction with obvious thermodynamic and spectroscopic consequences; these were not observed. We note in addition that it is possible to model a ps_{RR}–ps_{RY} junction without apparent stereochemical conflicts (12).

The thermodynamic analysis of the two component helices ps-GA_{15} and ps-F5·F6 and the 30 bp ps-L1·L2 provide an important means of studying the stability of two different ps structures within the same duplex. Both ps-GA_{15} and ps-F5·F6 have been shown previously and in the present study to melt in accordance with a two-state mechanism (13,29). ps-L1·L2 does not conform to this model, but exhibits a behavior consistent with the predictions of the more appropriate statistical mechanical treatment for a molecule with a chain length 30. One should emphasize that the number of fit parameters in Models 1 and 2 are the same (excluding the additional nucleation factor in Model 2, the specification of which does not appreciably affect the global parameters). Although the statistical mechanical formalism for the helix–coil equilibrium (40) has been available for more than 30 years, it is not usually applied to the evaluation of oligonucleotide melting data. In the present instance, the combined analyses led us to the conclusion that both individual ps structures are retained in the joint duplex molecule, without perceptible destabilization due to the intervening junction. This interpretation was confirmed by chemical modification with DEPC, in which a significant decrease in reactivity was observed upon formation of the ps duplex relative to the single-stranded form, with no evidence for hyperreactivity at the junctional region.

A number of alternative base pairing schemes for ps_{RR}-DNA have been proposed and are currently under investigation (8,12,13). The polymorphic repertoire of the $d(GA)_n$ sequence comprises a number of distinct secondary structures. For example, under acid conditions, an aps hairpin with d(G·A) base pairs stabilized by a terminal segment of Watson–Crick base pairs (46) as well as an ordered single-stranded structure (47) have been proposed. It is important to stress that the ps_{RR}-DNA conformation of alternating $d(GA)_n$ studied here and previously (13) is clearly a duplex structure unrelated to the tetraplex proposed for polymeric DNA (48). It is stable at neutral pH, i.e. in the absence of hemi-protonated cytosine, and is preferentially stabilized by Mg^{2+} (13,37). In addition, it has been shown that a ps_{RR} duplex with the sequence motif $d(GAAGGA)_n$ is less stable than the strictly alternating duplex of the same length (13), suggesting a dinucleotide repeat as the preferred structural unit. Thus, any model proposed for ps-$d(GA)_n$ must take into account the preferential stabilization by divalent cations, incorporate a dinucleotide repeat element, and provide for a smooth transition to a ps_{RY} helix.

As we learn more about the structural flexibility of DNA, it becomes increasingly apparent that a wide variety of structural motifs may have biological functions in living systems. Guanine-rich sequences are an excellent example of such polymorphic DNA. For example, an RNA polypurine segment in the retroviral 'dimer linkage structure' (DLS) has been implicated in the dimerization of a fragment from the HIV-1 genome via quadraplex formation (49,50). The DLS is responsible for the parallel alignment of the two RNA strands comprising the viral genome (51). Duplex ps_{RR}-RNA may also be involved (12,32,37). Both structural elements, in the form of a ps_{RR}-RNA·DNA hybrid (12) and a quadruplex (3) have been suggested as intermediates in the regulation of the immunoglobulin (IgA) switch regions of lymphocytes. Inasmuch as such features cannot exist in isolation but rather as part of a larger chromosomal unit, the combination of ps duplex and tetraplex elements could provide a mechanism for selective pairing and stereochemical alignment. The 30 bp ps-L1·L2 duplex may serve as a model for these situations. Other functions have been proposed for ps-DNA in gene expression, recombination, RNA processing (14,18,20), the packing of single-stranded and dimeric viral genomes and the function of reverse gyrase (12). The significant conclusion of this work is that two ps conformations that possess distinct secondary structure and sequence requirements for formation, can coexist stably within a single duplex. The two helical regions incorporate 3 out of the 4 natural bases and can be juxtaposed without significant mutual destabilization or perturbation. However, the precise nature of the intervening junction remains to be established.

The existence of parallel-stranded DNA and the numerous other manifestations of DNA polymorphism raise the question as to what constitutes the essential nature of the DNA molecule. The enzymatic mechanism of semi-conservative replication based on the canonical Watson–Crick base pairs ensures that the bulk of cellular DNA corresponds to the classical B conformation. However, from a physicochemical standpoint, many of the known

alternative structures, including those discussed in this report, exhibit higher stability under certain circumstances (ionic environment, ligand and protein binding). Thus, once uncoupled from the processes of replication and transcription, in which one assumes that only B-DNA serves as a template, DNA and RNA may engage in cellular functions dictated by structural features unrelated to the primary genetic message.

ACKNOWLEDGEMENTS

The authors wish to thank Ms Gudrun Heim for excellent technical assistance, and Drs Vitaly Kuryavyi and Dorus Gadella for valuable discussions. E.M.E. is the recipient of a postdoctoral fellowship from the Alexander von Humboldt Foundation.

REFERENCES

1. Aboul-ela, F., Murchie, A.I.H. and Lilley, D.M.J. (1992) *Nature*, **360**, 280–282.
2. Sarma, M.H., Luo, J., Umemoto, K., Yuan, R.D. and Sarma, R. (1992) *J. Biomol. Struct. Dyn.*, **9**, 1131–1153.
3. Sen, D. and Gilbert, W. (1988) *Nature*, **334**, 364–366.
4. Zimmerman, S.B., Cohen, G.H. and Davies, D.R. (1975) *J. Mol. Biol.*, **92**, 181–192.
5. Rich, A., Davies, D.R., Crick, F.H.C. and Watson, J.D. (1961) *J. Mol. Biol.*, **3**, 71–86.
6. Langridge, R. and Rich, A. (1963) *Nature*, **198**, 725–728.
7. Luo, J., Sarma, M.H., Yuan, R. and Sarma, R.H. (1992) *FEBS Lett.*, **306**, 223–228.
8. Robinson, H., van der Marel, G.A., van Boom, J.H. and Wang, A.H.-J. (1992) *Biochemistry*, **31**, 10510–10517.
9. Jovin, T.M., Rippe, K., Ramsing, N.B., Klement, R., Elhorst, W. and Voijtiskova, M. (1990) In Sarma, R.H. and Sarma, M.H. (eds), *Structure & Methods*, Vol. 3, *DNA & RNA*. Adenine Press, Schenectady, NY, pp. 155–174.
10. Jovin, T.M. (1991) In Eckstein, F. and Lilley, D.M. (eds), *Nucleic Acids and Molecular Biology*. Springer-Verlag, Berlin, Vol. 5, pp. 25–38.
11. Rippe, K. and Jovin, T.M. (1992) *Methods Enzymol.*, **211**, 199–220.
12. Rippe, K., Kuryavyi, V.V., Westhof, E. and Jovin, T.M. (1992) In Lilley, D.M.J., Heumann, H. and Suck, D. (eds), *Structural Tools for the Analysis of Protein–Nucleic Acid Complexes. Advances in Life Sciences (ALS)*. Birkhäuser Verlag, Basel, Switzerland, pp. 81–107.
13. Rippe, K., Fritsch, V., Westhof, E. and Jovin, T.M. (1992) *EMBO J.*, **11**, 3777–3786.
14. Kuryavyi, V.V. (1987) *Molekulyarnaya Biologiya*, **21**, 1486–1496.
15. Il'ychova, I.A., Lysov, Y.P., Chernyi, A.A., Shchyolkina, A.K., Gottikh, B.P. and Florentiev, V.L. (1990) *J. Biomol. Struct. Dyn.*, **7**, 879–897.
16. Pattabiraman, N. (1986) *Biopolymers*, **25**, 1603–1606.
17. van de Sande, J.H., Ramsing, N.B., Germann, M.W., Elhorst, W., Kalisch, B.W., v. Kitzing, E., Pon, R.T., Clegg, R.M. and Jovin, T.M. (1988) *Science*, **241**, 551–557.
18. Ramsing, N.B. and Jovin, T.M. (1988) Nucleic Acids Res., **16**, 6659–6676.
19. Germann, M.W., Kalish, B.W. and van de Sande, J.H. (1988) *Biochemistry*, **27**, 8302–8306.
20. Tchurikov, N.A., Chernov, B.K., Golova, Y.B. and Nechipurenko, Y.D. (1989) *FEBS Lett.*, **257**, 415–418.
21. Tchurikov, N.A., Shchyolkina, A.K., Borissova, O.F. and Chernov, B.K. (1992) *FEBS Lett.*, **297**, 233–236.
22. Rippe, K., Ramsing, N.B. and Jovin, T.M. (1989) *Biochemistry*, **28**, 9536–9541.
23. Rippe, K., Ramsing, N.B., Klement, R. and Jovin, T.M. (1990) *J. Biomol. Struct. Dyn.*, **7**, 1199–1209.
24. Förtsch, I., Zimmer, C., Birch-Hirschfeld, E., Evertsz, E. and Jovin, T.M., manuscript in preparation.
25. Rippe, K. and Jovin, T.M. (1989) *Biochemistry*, **28**, 9542–9549.
26. Ramsing, N.B., Rippe, K. and Jovin, T.M. (1989) *Biochemistry*, **28**, 9528–9535.
27. Klysik, J., Rippe, K. and Jovin, T.M. (1990) *Biochemistry*, **29**, 9831–9839.
28. Otto, C., Thomas, G.A., Rippe, K., Jovin, T.M. and Peticolas, W.L. (1991) *Biochemistry*, **30**, 3062–3069.
29. Rentzeperis, D., Rippe, K., Jovin, T.M. and Marky, L.A. (1992) *J. Am. Chem. Soc.*, **114**, 5926–5928.
30. Rippe, K., Dötsch, V. and Jovin, T.M. (1994) In Funck, T. (ed.), *DNA, Interaction wth Ligands and Proteins. Problems of Recognition and Self-organization. Fundamental Aspects and Technical Trends*. Nova Science, Commack, NY, in press.
31. Fritzsche, H., Akhebat, A., Taillandier, E., Rippe, K. and Jovin, T.M. (1993) *Nucleic Acids Res.*, **21**, 5085–5091.
32. Rippe, K. and Jovin, T.M., manuscript in preparation.
33. Loontiens, F.G. and Jovin, T.M., unpublished results.
34. Zhou, N., Germann, M.W., van de Sande, J.H., Pattabiraman, N. and Vogel, J.J. (1993) *Biochemistry*, **32**, 646–656.
35. Germann, M.W., Kalish, B.W., Pon, R.T. and van de Sande, J.H. (1990) *Biochemistry*, **29**, 9426–9432.
36. Shchyolkina, A.K., Lysov, Y.P., Il'ychova, I.A., Chernyi, A.A., Golova, Y.B., Chernov, B.K., Gottikh, B.P. and Florentiev, V. L (1989) *FEBS Lett.*, **244**, 39–42.
37. Evertsz, E.M. and Jovin, T.M., unpublished results.
38. Marky, L.A. and Breslauer, K.J. (1987) *Biopolymers*, **26**, 1601–1620.
39. Longfellow, C.E., Kierzek, R. and Turner, D.H. (1990) *Biochemistry*, **29**, 278–285.
40. Applequist, J. and Damle, V. (1963) *J. Chem. Phys.*, **39**, 2719–2721.
41. Petersheim, M. and Turner, D.H. (1983) *Biochemistry*, **22**, 256–263.
42. Puglisi, J.D. and Tinoco, I.J. (1989) *Methods Enzymol.*, **180**, 304–325.
43. Breslauer, K.J., Frank, R., Blöcker, H. and Marky, L.A. (1986) *Proc. Natl. Acad. Sci. USA*, **83**, 3746–3750.
44. Scheffler, I.E., Elson, E.L. and Baldwin, R.L. (1970) *J. Mol. Biol.*, **48**, 145–171.
45. Lee, J.S., Johnson, D.A. and Morgan, A.R. (1979) *Nucleic Acids Res.*, **6**, 3073–3091.
46. Huertas, D., Bellsolell, L., Casanovas, J.M., Coll, M. and Azorin, F. (1993) *EMBO J.*, **12**, 4029–4038.
47. Dolinnaya, N.G. and Fresco, J.R. (1992) *Proc. Natl. Acad. Sci. USA*, **89**, 9242–9246.
48. Lee, J.S. (1990) *Nucleic Acids Res.*, **18**, 6057–6060.
49. Awang, G. and Sen, D. (1993) *Biochemistry*, **32**, 11453–11457.
50. Sundquist, W., I. and Heaphy, S. (1993) *Proc. Natl. Acad. Sci. USA*, **90**, 3393–3397.
51. Kung, H.-J., Hu, S., Bender, W., Bailey, J.M., Davidson, N., Nicolson, M.O. and McAllister, R.M. (1976) *Cell*, **7**, 609–620.